Energy transfer in quasibinary and collective scattering events at a Ag(001) surface

M. P. Ray, R. E. Lake, and C. E. Sosolik*
Department of Physics and Astronomy, Clemson University, Clemson, South Carolina 29634, USA
(Received 19 December 2008; published 28 April 2009)

We have measured the in-plane scattered distributions of K^+ ions incident on a Ag(001) surface with energies from 9 to 100 eV. Energy- and angle-resolved spectra of the scattered flux show multiple peaks distinctly separated in energy corresponding to specific ion trajectories at the surface. Using a calculated interaction potential combined with the classical scattering simulation SAFARI we are able to model these trajectories and detail their energy-loss characteristics. At energies below approximately 24 eV we find that the ions scatter with a larger energy than one would expect from quasibinary collisions. Our trajectory analysis reveals this is a transition from the quasibinary behavior to a collective surface response more commonly associated with thermal energy atom scattering.

DOI: 10.1103/PhysRevB.79.155446 PACS number(s): 68.49.Sf, 34.50.−s, 34.35.+a, 79.20.Rf

I. INTRODUCTION

Hyperthermal energy ion scattering measurements at surfaces have long been used to probe the repulsive or hard-wall interatomic potential between the surface and scatterer.[1–5] Alkali ion scattering from metal surfaces are ideal systems for such studies. The noble-gas electronic structure of singly ionized alkalis simplifies the construction of the interaction potential and the well-understood electronic behavior simplifies the interpretation of the energy spectra. Although previous work has shown that in the hyperthermal energy regime, an interaction potential that is summed over several surface atoms is required to match the experimental results, the scattered spectra have always been described as sequential *quasibinary* collisions between the ion and the surface atoms. The results contained in this work represent a quantitative study[6,7] of collective effects that are not quasibinary in nature.

Prior work focused on scattering phenomena at these energies was carried out by Cooper and co-workers[8–13] using alkali ion beams in the Cu(110) and Cu(100) systems, however collective effects were never observed in these studies. In this paper we present a detailed study of the scattering dynamics and interaction potential for hyperthermal (9–100 eV) K^+ scattering from Ag(001). Using experimental results combined with simulations we are able to study the scattering dynamics as well as extract an interaction potential for the K^+-Ag(001) system. We present energy- and angle-resolved scattering distributions and compare them to simulations using a model potential that includes an attractive image term. Using the calculated potential we are able to accurately model the evolution of the scattered energy distribution as a function of incident energy. For the lowest energies used in this work we found that collective effects must be considered to interpret the data.

The paper is organized as follows. First, we describe the experimental setup used to produce the hyperthermal energy beams and experimental technique (Sec. II). A discussion of the data, the classical scattering simulation SAFARI (Ref. 14) and the model potentials, follows. Then, we present energy- and angle-resolved data and compare them to results from SAFARI to identify trajectories that correspond to peaks in the measured energy spectra (Secs. II and III). Finally, we summarize our results (Sec. IV).

II. EXPERIMENTAL TECHNIQUES

Both the hyperthermal energy ion source and the crystal surface utilized in the measurements reported here were mounted in a unique ultrahigh vacuum (UHV) scattering system.[15] The source consists primarily of a Colutron G-2 ion gun.[16] For our measurements, a home-built source[17] that incorporates a commercially available potassium-doped aluminosilicate emitter[18] is used to produce our K^+ ions. The ions are scattered from the target in a two-tier UHV chamber that houses various surface analysis tools, two scattered particle detectors, and a six-axis manipulator stage. The upper tier of the scattering chamber contains sample analysis instruments including a sputter gun, Auger-electron spectrometer, Kelvin probe, and a low energy electron diffraction setup. The ion detector is located in the lower tier of the scattering chamber. The detector lies in plane with the incident ion beam. The ion detector uses a 180° electrostatic analyzer (ESA) and channel electron multiplier to detect ions with an energy resolution of 1%.

The sample target is a 10 mm diameter hat-shaped Ag(001) single crystal obtained from MaTecK.[19] In preparation for the scattering experiments, sputter and anneal cycles were performed for cleaning the sample. Each cycle consisted of exposure to a 500 eV Ar^+ beam for 20 min followed by annealing at 420 °C for 10 min. Sample cleanliness was verified using Auger-electron spectroscopy. Also, surface order and the scattering azimuth were verified via low energy electron diffraction.

Following each cleaning cycle, the room-temperature crystal was exposed to a K^+ beam and ions scattered from the surface were detected using the ESA. A typical spectrum is shown in Fig. 1, where the scattered intensity is plotted versus the scattered ion energy. For all spectra obtained here, the number of scattered ions detected at each ESA pass energy is obtained by summing counts during a predetermined dwell time of 5 s. In addition, the counts obtained at each pass energy have been multiplied by $1/E$ to account for the transmission function of the ESA. The pressure in the scat-

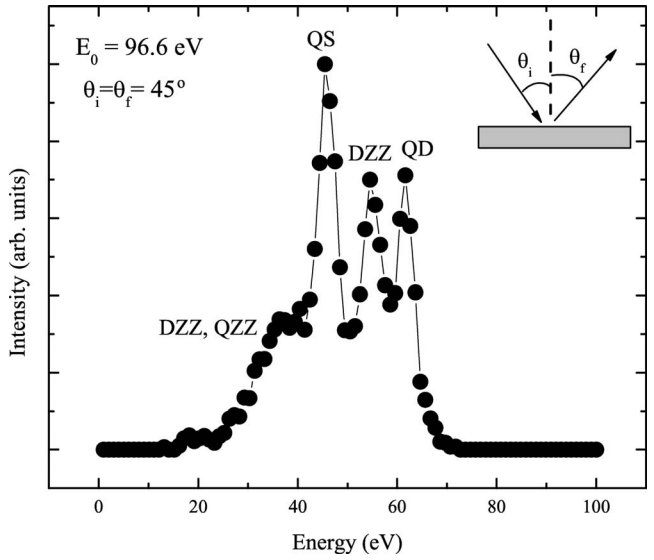

FIG. 1. A representative energy-resolved spectrum showing K^+ ions detected after scattering from a Ag(001) crystal along the ⟨110⟩ azimuth at an incident energy and angle of 96.6 eV and 45°, respectively. Inset depicts the scattering geometry used in the experiment. The line connecting successive data points is included to guide the eyes.

tering chamber during the experiment was typically in the high 10^{-10} Torr range.

Spectra were obtained for K^+ ions scattered from the Ag(001) surface at incident energies between approximately 9 and 100 eV. The K^+ ions were scattered from the single-crystal Ag(100) target along the ⟨110⟩ crystal azimuth at an incident angle of $\theta_i=45°$ with respect to the surface normal. In the representative data taken at $\theta_f=45°$ in Fig. 1, four well-defined peaks that correspond to significant energy losses are clearly resolved. One or more of these peaks are observed consistently across our range of final scattered angles. In the sections that follow we will examine the trajectories that make up these data and their evolution as a function of angle and incident energy.

III. RESULTS AND DISCUSSION

In the incident energy regime used here, the simplest description of our observed scattering data would employ the binary collision approximation (BCA), which relies on conservation of energy and momentum. Within the BCA, the kinematic factor, k, gives the ratio of the final and incident energies of a projectile ion $(\frac{E_f}{E_0})$ following a single collision with a target surface atom as

$$k(\mu,\theta_{\mathrm{TSA}})=\frac{\mu^2}{(1+\mu)^2}\left[\cos\,\theta_{\mathrm{TSA}}+\left(\frac{1}{\mu^2}-\sin^2\,\theta_{\mathrm{TSA}}\right)^{1/2}\right]^2. \quad (1)$$

This factor is a function of the projectile-to-target mass ratio $\mu=\frac{m_{\mathrm{proj}}}{m_{\mathrm{target}}}$ and the total scattering angle, $\theta_{\mathrm{TSA}}=180°-\theta_i-\theta_f$. For the K^+-Ag(001) scattering data shown in Fig. 1, two in-plane trajectory types are easily identified using this formalism. Specifically, the peak labeled as quasisingle (QS) coincides with a single K^+-Ag collision and has a calculated final energy of 45 eV or $k=0.468$. Additionally, the peak labeled as quasidouble (QD) has a calculated final energy of 63 eV and a "combined" kinematic factor of 0.649. The QD peak corresponds to a trajectory where a K^+ ion scatters sequentially from two Ag atoms and travels parallel to the surface plane along the ⟨110⟩ direction between the collisions. As such, the QD trajectory is described by the product of two identical kinematic factors, i.e., $k(\mu,\theta_{\mathrm{TSA}}=90°)^2$ for the data shown in Fig. 1.

Although the BCA is able to predict the peak positions for both QS and QD trajectory types, it is clear other trajectories must be present in the data of Fig. 1. These trajectories, which are more complex and typically out of plane, are not readily calculated within the BCA. In addition, the BCA makes no allowance for the relative intensities observed for different trajectories at a given energy and offers no straightforward mechanism for following the evolution of allowed or nonallowed trajectories as the incident energy is varied. To identify and follow all allowed trajectories as a function of incident energy and angle, a simulation method is required that incorporates a realistic ion-surface potential and that models the surface crystal structure. Although standard simulations such as TRIM (Ref. 20) and KALYPSO (Ref. 21) are possible solutions, neither is designed for the hyperthermal energy regime nor is able to reproduce our experimental data. Therefore, we have employed the simulation SAFARI to interpret these data.

Within SAFARI, it is assumed that the energy loss for a scattered ion is due solely to momentum transfer to the recoiling surface atoms. Although one could consider additional energy-loss channels such as electron-hole pair formation, the typical losses to this channel are less than a few tenths of an eV for ions interacting with metals at our velocities.[22–25] Such small contributions would not alter our results and are therefore not included in the present simulations.[26] In the sections that follow, we describe the ion-surface interaction potential that is used to model scattering for this system (Sec. III A), the trajectory types that were found to match our data within SAFARI (Secs. III B and III C), and the unexpected role that collective surface interactions play in determining the scattered distribution at our lowest incident energies (Sec. III D).

A. Interaction potential

In order to compute the forces that act between the incident K^+ ion and the Ag crystal within SAFARI a user-defined interaction potential is required. Based on previous alkali ion-surface studies,[8,9] we have constructed an ion-surface potential that is a sum of repulsive pair potentials with an additional attractive term included to account for the image interaction. Explicitly, we take the full repulsive term to be the sum of the individual repulsive contributions from the n nearest Ag atoms to the K^+ ion, $V_{\mathrm{rep}}(r)=\Sigma_{i=1}^{n}V_{\mathrm{pair}}(r_i)$. By forming the repulsive term in this way, it is possible to vary the number of "interacting" or nearest-neighbor Ag atoms at the surface during a simulated scattering event. As we show

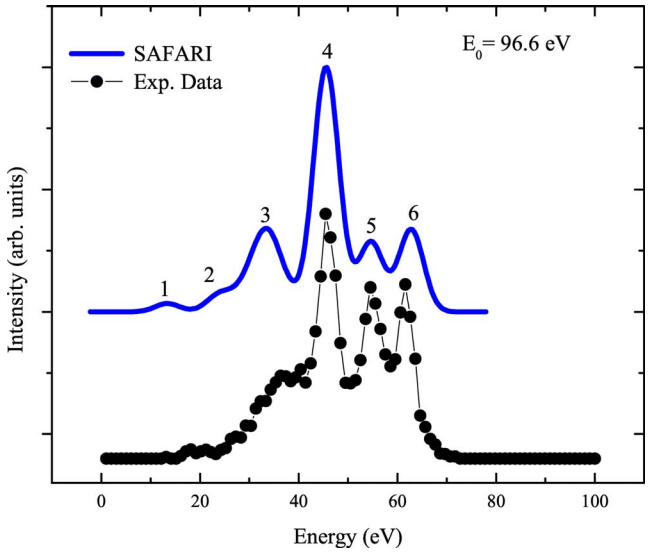

FIG. 2. (Color online) Measured and simulated energy spectra are compared for ions scattered specularly at 45°. The interaction potential described in the text is used and the surface is modeled to be at 0 K. Each peak in the simulated spectrum is numbered and associated with the trajectories depicted in Fig. 3.

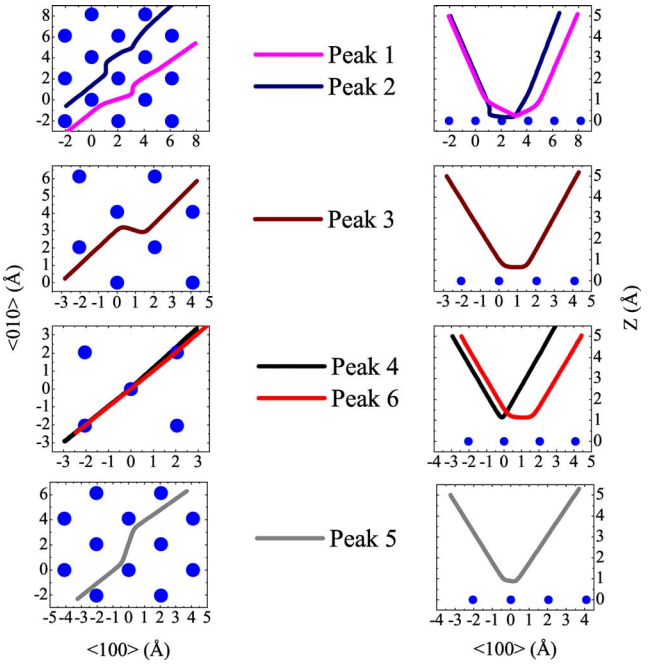

FIG. 3. (Color online) Top and side views of the ion trajectories. The left side represents a top view with lines representing the ion trajectories and the circles depict the surface atoms. Peaks 1 and 2 are the QZZ trajectories, 3 and 5 are the DZZ trajectories, and 4 and 6 are the QS and QD trajectories, respectively.

in Sec. III D, this allows us to isolate specific collective or multiatom effects that are responsible for the trajectories contained in our scattered spectra.

The individual repulsive term $V_{\text{pair}}(r)$ we use here is a calculated Hartree-Fock pair potential. Although other universal forms for the repulsive term are often used in low energy ion scattering simulations, in particular the Ziegler-Biersack-Littmarck potential,[27] previous work has shown that these fail in the hyperthermal energy regime.[9] Our single repulsive pair term was found by first calculating the ground-state energy of an isolated K-Ag dimer with interatomic separations between 0.5 and 2.0 Å. The isolated ground-state energies of individual K and Ag atoms were then calculated and subtracted from these dimer values to isolate the repulsive contribution to the energy, i.e., $V_{\text{pair}}(r) = E[\text{K-Ag}](r) - E[\text{K}] - E[\text{Ag}]$. The values for $V_{\text{pair}}(r)$ were all calculated using the Hartree-Fock code in the quantum chemistry package GAUSSIAN 98.[28]

The attractive bulk interaction that arises due to the image charge formed in the metal was represented within SAFARI as a z dependent function

$$V_{\text{attr}}(z) = -e^2/\sqrt{16(z-z_0)^2 + e^4/V_{\text{min}}^2}, \tag{2}$$

where z is the perpendicular distance from the top layer of Ag surface atoms. Written in this way, $V_{\text{attr}}(z)$ is saturated to V_{min} close to the surface and tends smoothly to $1/4z$ for large values of z. V_{min} and z_0 determine the depth of the image well and are the only adjustable parameters in the total potential. For this work z_0 was taken to be 1.26 Å from the atomic cores[29] and a V_{min} value of 0.5 eV was found to give the best agreement with the experimental data. An example of a simulated spectrum obtained using the full interaction potential described here is shown in Fig. 2 for $E_0 = 96.6$ eV.

B. Trajectory analysis

A comprehensive analysis of the individual scattering events or trajectories that give rise to the energy-resolved peaks within all spectra across our incident energy range of 9–100 eV has revealed three main results. First, the scattering in this energy range occurs almost entirely from first layer atoms. This result is consistent with previous studies and reinforces the need for including the actual Ag(001) crystal structure in the simulation. Second, along with the in-plane QS and QD trajectory types, there are three out-of-plane trajectory types present within our data. The relative position and occurrence of these trajectories within a given spectrum are energy and angle dependent (Sec. III C). Third, we find that as the incident energy is lowered and the apparent corrugation of the crystal surface decreases, complex out-of-plane trajectories become less probable. However, at the lowest incident energies where one would expect the image charge interaction to control the energy distribution, a collective scattering event dominates the scattered intensity (Sec. III D).

The experimental and simulated spectra taken at our highest incident energy and shown in Fig. 2 provide clearly resolved, well-defined peaks for a discussion of the trajectory types seen across our full incident energy range. The simulated peaks, labeled 1–6, contain the four trajectory types shown in Fig. 3. The simplest trajectories, present in peaks 4 and 6 of Fig. 2, are the QS and QD trajectories, respectively. We note that the prefix *quasi-* is included when describing these and other events because a scattered K^+ ion can in fact interact with multiple surface atoms along its trajectory. The

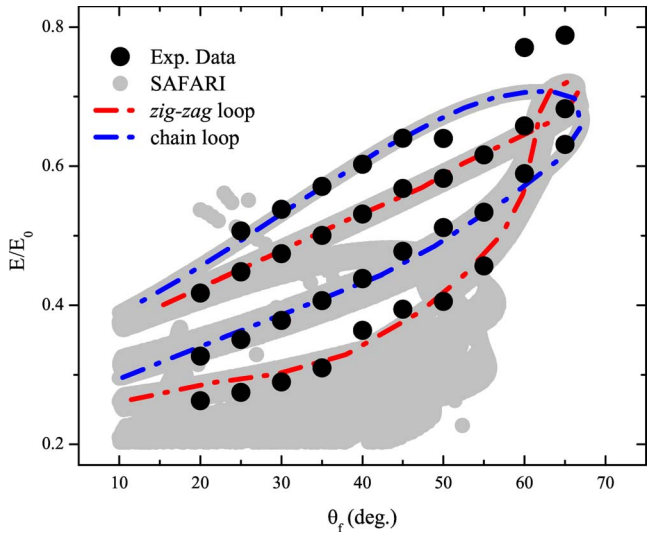

FIG. 4. (Color online) A comparison between the data and the simulation using the total interaction potential for detector angles ranging from 20° to 65°. The chain loop results from impact parameters lying along the ⟨110⟩ azimuth and the zig-zag loop is caused by trajectories that scatter in the ⟨110⟩ channel. The low energy-loss peaks at θ_f of 60° and 65° are the result of scattering from a room-temperature crystalline sample (see text).

more complex trajectories beyond the QS and QD types can be grouped into two types. The first, present in peaks 1 and 2 of Fig. 2, corresponds to quadruple *zig-zag* (QZZ) trajectories. In these events shown in Fig. 3 the K^+ ion undergoes four small-angle collisions at the surface as it travels along a channel in the ⟨110⟩ direction. The difference in energy between events in peaks 1 and 2 is caused by the different impact parameters involved in the initial surface collisions for each trajectory. That is, although an ion strikes the same number of surface atoms in both cases, the scattering centers and hence the energy losses differ giving rise to distinct peaks in the simulated spectrum. This particular trajectory type has not been observed in other alkali ion-surface experiments performed in this energy range. The second type of complex trajectory is present in peaks 3 and 5 and corresponds to double zig-zag (DZZ) trajectories where the ion strikes two surface atoms across the ⟨110⟩ channel from one another. As in the case of the QZZ trajectories, the final scattered energy for a particular DZZ trajectory is determined by the initial impact parameter. Peak 3 represents ions in a DZZ trajectory where the second target atom is directly across the ⟨110⟩ channel from the initial target atom, while in peak 5, the second atom is located diagonally across the ⟨110⟩ channel. The large-angle scattering event that makes the DZZ of peak 3 possible also inherently involves a large energy loss, which explains the energetic separation of the two otherwise similar DZZ trajectories.

C. E-θ_f comparison

As a rigorous test of our calculated K^+-Ag interaction potential and the trajectories simulated within SAFARI, we present the angle-resolved data set or E-θ_f plot of Fig. 4. The experimental results presented here consist of multiple energy-resolved spectra, where each spectrum has been fit to a sum of Gaussian terms. The peak positions extracted from these fits are plotted as a function of the detection angle (θ_f) over the range of 20°–65°. The SAFARI-simulated data are represented here first as a series of two overlapping loop structures shown as dashed lines and second as a gray-scaled background showing the full E/E_0 region that is predicted to lead to a minimum scattered intensity. As such, the loops (dashed lines) are representative of the maximum scattered intensity and are expected to correspond most closely to the peak position we have extracted from our fits to the experimental data.

The general agreement present in Fig. 4 between the simulated and the experimental data demonstrates that the interaction potential we have constructed is valid across our range of accessible θ_f values. Looking more closely, we note that the observed trend in both data sets as a function of increased θ_f is toward an increase in the final scattered energy. This is understandable qualitatively based on the fact that larger θ_f values correspond to smaller total angular deflections for an interacting ion and hence collisions or trajectories that involve progressively lower energy loss. The presence of the looplike structures (labeled chain and zig-zag) is consistent with previous results on alkali ion-surface systems[9,11] and is indicative of crystalline order at the surface of our Ag(001) sample. Moreover, the matching of the loop structures seen between the experimental and simulated data further indicate the accuracy of our calculated potential, since it is the detailed corrugation of the crystal lattice that gives rise to these loops. A deviation is seen between the two data sets, however, at the largest θ_f values. This is an expected deviation from perfect crystalline order that one should observe in a thermally vibrating surface.[30,31] That is, in a perfect crystal there would be a merging of the trajectory types and a maximum in scattered intensity at the angular maxima or *rainbow* angles.[4,32,33] The fact that our data deviate at this point is a consequence of our Ag(001) sample being at room temperature during these measurements.

If we examine the loops more closely within SAFARI using single-shot trajectory analysis, we see that there are four distinct branches present over this θ_f range. These branches can be assigned to the trajectory types discussed in Sec. III B. In general, we find that the zig-zag loop represents the parameter space of impact points that lead to out-of-plane zig-zag trajectory types and that the chain loop is the basis of the chainlike QS and QD trajectories that scatter solely along the ⟨110⟩ azimuth. More specifically, we see that the low energy branch of the zig-zag loop is due to QZZ and DZZ trajectories, while the low energy branch of the chain loop is due to the QS trajectory. The upper or high energy branch of the zig-zag loop is due to the diagonal DZZ trajectory (peak 5 of Fig. 3), and the upper branch of the chain loop is due to the QD trajectory. The spreading of the intensity or the grayscale in Fig. 4 below the zig-zag loop and down to $\frac{E}{E_0} \sim 0.2$ is an indication of the many impact parameters that can lead to the QZZ and DZZ trajectory types. We see this spreading clearly in the data of Fig. 2, where peaks 1–3 represent an energy-broadened distribution to which a single peak has been fit within our $E-\theta_f$ plot of Fig. 4.

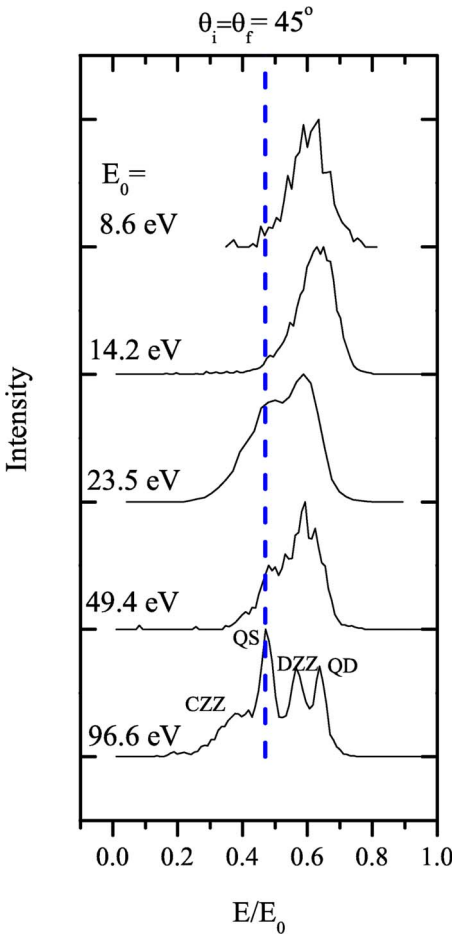

FIG. 5. (Color online) Scattered spectra for a range of incident energies are compared for a constant specular scattering geometry of 90°. For reference, the kinematic factor for a single binary collision is plotted as a dashed line at $E/E_0=0.47$. The label CZZ is given to the channel zig-zag trajectories which consist of the DZZ and QZZ trajectories. Each spectrum has been normalized by the incident energy (E_0) for comparison. For low incident energies the peaks shift to a higher energy due to collective surface-atom effects.

D. Collective scattering effects

We have found that the trajectory analysis discussed in Sec. III C is valid across our energy range down to $E_0 \sim 24$ eV. In Fig. 5, we show a series of specular spectra that span this range and it is clear that although the scattered peaks broaden due to thermal effects,[34] the scattered intensity is still localized in the region of the QS and QD peaks. Also, a reduced intensity from the QZZ and DZZ peaks in this energy range is observed, but this is expected since the penetration of an ion into the channel between parallel ⟨110⟩ chains of surface atoms becomes more difficult. For lower energies, however, the scattered intensity is clearly shifted away from the QS position and toward a higher energy. This is a somewhat counter-intuitive result, since one would expect that the image interaction would play a large role, possibly shifting *down* the scattered energy of any ions.

Trajectory analysis at $E_0 \sim 14$ eV and below shows that the dominant trajectory type within this lower energy range has become a modified DZZ-type trajectory that is qualitatively similar to peak 5 from Fig. 4. A comparison of a SAFARI spectrum and the experimental data at this energy is shown in Fig. 6. A systematic analysis within SAFARI finds that this result can only be reproduced if a *minimum* of two nearest Ag atoms ($n=2$) is included in the repulsive potential. This, in effect, rules out the possibility that the trajectory is instead a chainlike QD trajectory.

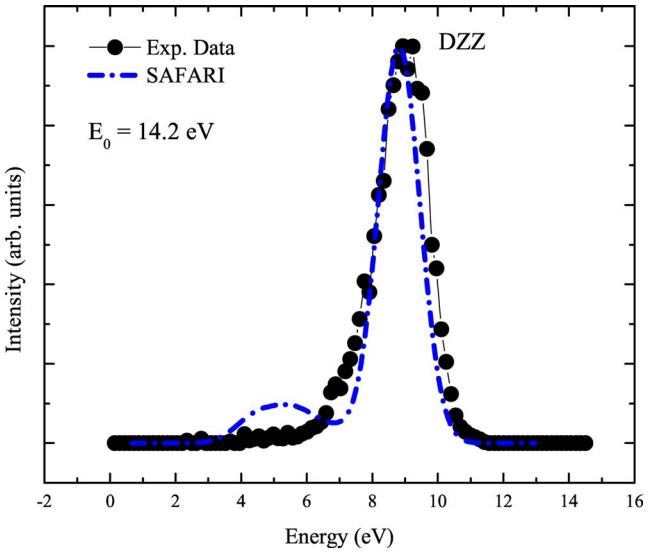

FIG. 6. (Color online) Measured and simulated energy spectra are compared for ions scattered specularly at 45°. With the exception of the incident energy, the interaction potential for this energy shares the same parameters as the higher energy spectrum in Fig. 1. The broadened low intensity peak at ~5 eV is due to QS and QD trajectories.

If we interpret the simulation qualitatively, it appears as if a K^+ ion undergoing this new DZZ trajectory is colliding with *two* Ag atoms simultaneously. This is distinctly different than the quasibinary nature of all the previous K-Ag collisions that made up the trajectories discussed above. In fact, a quantitative check on this result finds that a kinematic factor of $k=0.69$ can be obtained for scattering from two Ag atoms in this geometry, giving a reasonable value of $E=9.8$ eV for the spectrum of Fig. 6. This agreement is also present for $E_0=8.6$ eV and represents a quantitative example of a transition from the *quasibinary* nature of scattering trajectories commonly identified with hyperthermal energy ion scattering to the more *collective* surface response that is normally taken into account to describe scattering at lower, i.e., thermal energies.

IV. SUMMARY

We have measured energy- and angle-resolved spectra for hyperthermal energy K^+ scattered from the surface of Ag(001) along the ⟨110⟩ azimuth. The angle of incidence was fixed at 45° and the final angle of the detector was varied between 20° and 65°. In general the scattered spectra contained four distinct peaks indicating the presence of specific ion trajectories at the surface. To interpret these data we

calculated the repulsive portion of the interaction as a Hartree-Fock pair potential between the ion and surface atoms. An attractive potential was also included to model the image charge induced in the metal. Excellent agreement was found between the experimental and simulated data indicating the suitability of our potential parameterization for this hyperthermal energy regime.

We have also probed the transition from an ion undergoing multiple quasibinary surface collisions to the surface having a response that is collective and multiatom in nature. By holding the incident and final angles constant and reducing the incident energy, we find the energy transfer to be less than that expected from image charge effects alone. This observed increase in the relative scattered energy is found to arise from a collective surface response where the combined repulsive potentials of two surface atoms scatter a K^+ ion into our detector.

ACKNOWLEDGMENT

This work was supported by the National Science Foundation (Contract No. NSF-CHE-0548111).

*sosolik@clemson.edu

[1] B. H. Cooper and E. R. Behringer, *Low Energy Ion Surface Interactions* (Wiley, New York, 1994), pp. 263–312.
[2] A. D. Tenner, K. T. Gillen, A. W. Kleyn, and J. Los, Vacuum **33**, 665 (1983).
[3] P. J. van den Hoek, A. D. Tenner, A. W. Kleyn, and E. J. Baerends, Phys. Rev. B **34**, 5030 (1986).
[4] T. C. M. Horn, H. C. Pan, P. J. van den Hoek, and A. W. Kleyn, Surf. Sci. **201**, 573 (1988).
[5] A. W. Kleyn and T. C. M. Horn, Phys. Rep. **199**, 191 (1991).
[6] H. Lee and H. Kang, Bull. Korean Chem. Soc. **16**, 101 (1995).
[7] C. Kim, H. Kang, and S. C. Park, Nucl. Instrum. Methods Phys. Res. B **95**, 171 (1995).
[8] D. M. Goodstein, R. L. McEachern, and B. H. Cooper, Phys. Rev. B **39**, 13129 (1989).
[9] C. A. DiRubio, R. L. McEachern, J. G. McLean, and B. H. Cooper, Phys. Rev. B **54**, 8862 (1996).
[10] R. L. McEachern, D. M. Goodstein, and B. H. Cooper, Phys. Rev. B **39**, 10503 (1989).
[11] D. L. Adler and B. H. Cooper, Phys. Rev. B **43**, 3876 (1991).
[12] B. H. Cooper, C. A. DiRubio, G. A. Kimmel, and R. L. McEachern, Nucl. Instrum. Methods Phys. Res. B **64**, 49 (1992).
[13] E. R. Behringer, J. G. McLean, and B. H. Cooper, Phys. Rev. B **53**, 7510 (1996).
[14] D. M. Goodstein, S. A. Langer, and B. H. Cooper, J. Vac. Sci. Technol. A **6**, 703 (1988).
[15] M. P. Ray, R. E. Lake, S. A. Moody, V. Magadala, and C. E. Sosolik, Rev. Sci. Instrum. **79**, 076106 (2008).
[16] Colutron Research Corporation, Boulder, CO.
[17] D. R. Peale, D. L. Adler, B. R. Litt, and B. H. Cooper, Rev. Sci. Instrum. **60**, 730 (1989).
[18] HeatWave Labs, Inc., Watsonville, CA.
[19] MaTecK GmbH, Juelich, Germany.
[20] J. Biersack and L. Haggmark, Nucl. Instrum. Methods **174**, 257 (1980).
[21] M. Karolewski, Nucl. Instrum. Methods Phys. Res. B **230**, 402 (2005).
[22] F. Sols, P. Miranzo, and F. Flores, Surf. Sci. **161**, 33 (1985).
[23] J. E. Inglesfield, Surf. Sci. **127**, 555 (1983).
[24] J. B. Marston, D. R. Andersson, E. R. Behringer, B. H. Cooper, C. A. Di Rubio, G. A. Kimmel, and C. Richardson, Phys. Rev. B **48**, 7809 (1993).
[25] R. Brako and D. M. Newns, Rep. Prog. Phys. **52**, 655 (1989).
[26] The use of low and hyperthermal energy ions to probe electronic excitations in thin-film devices has recently generated considerable interest (Refs. 15 and 35–38).
[27] J. B. J. F. Ziegler and U. Littmark, *The Stopping and Ranges of Ions in Solids* (Pergamon, New York, 1985).
[28] M. J. Frisch *et al.*, GAUSSIAN 98, Revision A.7, Gaussian, Inc., Pittsburgh, PA, 1998.
[29] N. V. Smith, C. T. Chen, and M. Weinert, Phys. Rev. B **40**, 7565 (1989).
[30] B. Poelsema, L. K. Verhey, and A. L. Boers, Surf. Sci. **55**, 445 (1976).
[31] U. Gerlach-Meyer, E. Hulpke, and H. D. Meyer, Chem. Phys. **36**, 327 (1979).
[32] A. L. Boers, Surf. Sci. **63**, 475 (1977).
[33] V. E. Yurasova, V. I. Shulga, and D. S. Karpuzov, Can. J. Phys. **46**, 759 (1968).
[34] J. Powers, J. R. Manson, C. E. Sosolik, J. R. Hampton, A. C. Lavery, and B. H. Cooper, Phys. Rev. B **70**, 115413 (2004).
[35] S. N. Markin, D. Primetzhofer, S. Prusa, M. Brunmayr, G. Kowarik, F. Aumayr, and P. Bauer, Phys. Rev. B **78**, 195122 (2008).
[36] S. Meyer, D. Diesing, and A. Wucher, Phys. Rev. Lett. **93**, 137601 (2004).
[37] S. Meyer, C. Heuser, D. Diesing, and A. Wucher, Phys. Rev. B **78**, 035428 (2008).
[38] D. A. Kovacs, T. Peters, C. Haake, M. Schleberger, A. Wucher, A. Golczewski, F. Aumayr, and D. Diesing, Phys. Rev. B **77**, 245432 (2008).